



**HAL**  
open science

# Semi-numerical micromechanical model for viscoelastic microcracked masonry

Aida Chaker, Amna Rekik, André Langlet, Ridha Hambli

► **To cite this version:**

Aida Chaker, Amna Rekik, André Langlet, Ridha Hambli. Semi-numerical micromechanical model for viscoelastic microcracked masonry. *Mechanics of Materials*, 2022, 166, pp.104218. 10.1016/j.mechmat.2022.104218 . hal-03534189v1

**HAL Id: hal-03534189**

**<https://hal.science/hal-03534189v1>**

Submitted on 19 Jan 2022 (v1), last revised 7 Feb 2024 (v2)

**HAL** is a multi-disciplinary open access archive for the deposit and dissemination of scientific research documents, whether they are published or not. The documents may come from teaching and research institutions in France or abroad, or from public or private research centers.

L'archive ouverte pluridisciplinaire **HAL**, est destinée au dépôt et à la diffusion de documents scientifiques de niveau recherche, publiés ou non, émanant des établissements d'enseignement et de recherche français ou étrangers, des laboratoires publics ou privés.

# Semi-numerical micromechanical model for viscoelastic microcracked masonry

Aida Chaker<sup>a</sup>, Amna Rekik<sup>a,\*</sup>, André Langlet<sup>a</sup>, Ridha Hambli<sup>a</sup>

<sup>a</sup>*Univ. Orléans, Laboratoire de Mécanique Gabriel LaMé, Unité de recherche EA 7494, France*

---

## Abstract

This paper proposes a semi-numerical model providing accurate estimates for the mechanical behaviour of viscoelastic microcracked masonry. It relies on two steps. The first one approximates the creep behaviour of the microcracked mortar by coupling - in the Laplace-Carson symbolic space - the Griffith's theory to the Ponte-Castañeda & Willis (PCW) micromechanical scheme accounting for microcracks interactions and spatial distribution. The PCW model is an accurate alternative to the dilute and Mori-Tanaka model frequently used to homogenize microcracked media. Accumulated damage is assumed to follow a power-law time evolution according to the Weibull's failure rate function. In the second step, by contrary to the periodic homogenization technique adopted previously in [36] which approaches the masonry behaviour, finite elements method is used to model the complete geometry of the masonry and compute accurately (up to the numerical error) its local behaviour. The sensitivity of the proposed model to the mesh refinement is validated by comparison to analytical solution. It is worth noting that the proposed model accounts for creep of both brick and mortar constituents following the Generalized Maxwell rheological model. As a first illustration, the proposed model is applied to a compressed masonry wall. For the sake of simplicity, only mortar joints are assumed to be microcracked with frictionless open cracks. Comparisons between panels with elastic and viscoelastic bricks show the additional softening effect induced by the brick's creep increasing thus the risk of failure.

*Keywords:* Masonry, Creep, Microcracks, Laplace-Carson transform, Generalized Maxwell model, Ponte-Castañeda & Willis model, Finite element method

---

## 1. Introduction

In the last decades, masonry plays an important role in building thanks to its reasonable cost, durability and high resistance. According to the heterogeneity and nonlinear behaviour of its components, the numerical modeling of this composite becomes a real challenge. Various numerical models were developed in order to predict the global and local behaviours of masonry structures. In the literature, there are three modeling approaches. Firstly, in macro-models [1, 8, 9, 12, 34, 51], masonry constituents (bricks, mortar and brick/mortar interfaces) are smoothed out into a homogeneous continuum material. This approach requires a preliminary mechanical characterization of the model based on experiments. Secondly, the simplified micro-models [6, 38, 39], where the mortar and the brick/mortar interface are lumped into a common element, reduce the computational time even if some precision is lost. Finally, the detailed micro-modeling approach [27, 28, 52], modeling separately the mortar joint and the interface, is more accurate than the simplified one even it is more expensive in terms of computational time. Since, the masonry can be considered as an heterogeneous composite, it is noticed that some of the developed models consider elastic constituents [2, 24, 35], by contrary to others taking into account the nonlinear behaviour of these constituents such as plasticity [45, 50]. Nonetheless, the creep effect of each component on the masonry behaviour is generally neglected. Recently, several analytical and numerical studies were developed [10, 17, 16, 47] to evaluate the

---

\*Corresponding author

*Email address:* amna.rekik@univ-orleans.fr (Amna Rekik)

masonry creep behaviour at the undamaged state. For example, Baraldi and Cecchi [3] applied the discrete elements method to estimate the mechanical behaviour of a masonry wall subjected to compressive and shear loadings. While, bricks are assumed to be rigid, the mortar was considered to be viscoelastic following the Generalized Maxwell (GM) rheological model. The obtained results were validated by comparison with analytical solution available for a homogeneous plate [15]. The majority of the previous quoted papers neglect the brick's creep effect. Lenczner and Salahuddin [25] and Sayed-Ahmed et al. [41] proved through creep tests carried out on brickwork walls, that by contrary to the mortar's creep effect which presents almost 60 % to 80% of the total masonry creep, bricks are the origin of 20% of this total creep. Accordingly, brick's creep should not be neglected as proposed in this work. On the other hand, several rheological models were adopted in the literature to model the mortar creep behaviour such as Burgers, Feng, Ross and USBR models [23, 49, 48]. According to experimental tests carried out by Choi et al. [19], it was proved that the MM model describes well the mortar creep phenomenon better than other models. For this reason, the MM's model, which coincides with the Zener (a particular case of the Generalized Maxwell rheological model as a connection in parallel of a Maxwell element and a spring), will be used in this work as previously done in Rezik et al. [36, 37]. It is worth noting that few works are devoted to the combined effects of damage and creep in masonry even though presence of microcracks due to creep or external conditions (temperature, moisture, humidity, etc.) is a possible origin for the masonry collapse. Among works considering mortar damage, it is possible to quote Fan et al. [22] paper which proposed a 3D finite elements model based on analytical crack approach [46] to estimate the composite masonry column response under compressive loads. Other approach [30, 31, 29, 32, 33, 36, 37, 40, 43] consists to apply homogenization techniques in the Laplace-Carson space in order to assess the microcracked mortar's effective (or global) properties. This allows to substitute the heterogeneous mortar by a homogeneous equivalent material (HEM) which properties depend on crack density [11, 21] and time. Finally, the masonry's behaviour is estimated due to periodic homogenization technique [36, 37] using finite elements method (FEM). It is worth noting that Rezik's et al. model [40] was improved by substituting the dilute scheme (equivalent to the Mori-Tanaka model for microcracked material problems with stress boundary conditions [20]) by the PCW one which accounts for microcracks interactions and spatial distribution [36]. The present work replaces the periodic homogenization procedure by the modeling of the masonry's complete geometry and the accurate computation (up to numerical error) of its local behaviour due to the finite elements method. Moreover, the proposed model accounts for creep of both constituents: bricks and mortar.

This paper is organized as follows. The first section describes the main principle and steps on which relies the proposed model. The second part validates the semi-numerical model by comparison with analytical solution available in the literature for a homogeneous plate. At last, the relevance of the proposed model to predict mechanical local fields is illustrated by investigating the case of a masonry wall (with elastic and viscoelastic bricks) subjected to sustained compression loads.

## 2. Principle of the proposed multi-level model

The proposed model aims to provide accurate estimates for the mechanical response of viscoelastic microcracked masonry structures. It improves on the earlier model [36] since it computes "exactly" (up to numerical error) the damaged masonry behaviour instead of carrying out periodic homogenization technique which approximates the masonry effective behaviour. Notice that the herein proposed model is based on two steps. The first one is identical to that followed by the micromechanical model proposed by Rezik in [36]. It consist in substituting the viscoelastic microcracked mortar by a homogeneous equivalent material (HEM) which behaviour depends on time and crack density. Recall that this step relies on the coupling between the brittle Griffith's theory and linear homogenization technique [7]. In the symbolic space using the Laplace-Carson Transform (LCT), the mortar apparent behaviour is linear elastic. Again, according to the linear relation between the macroscopic stress and the displacement's jump induced by the crack [21], the mortar effective (or macroscopic) properties could be estimated, in the symbolic space, by the Ponte-Castañeda and Willis (PCW) model [14] which is a rigorous scheme allowing to account for microcracks interactions and their spatial distribution effect. Creep coefficients of the mortar's HEM were identified at short and long terms assuming that microcracked mortar follows also the MM's model as it is the case for

the undamaged mortar. This identification procedure was detailed in [40]. In the second step, different from that followed in [36], it is proposed here to compute accurately (up to numerical error) the local response of masonry using finite elements method. This avoids approximations related to the periodic homogenization procedure. The above mentioned steps are illustrated in Figure-1.

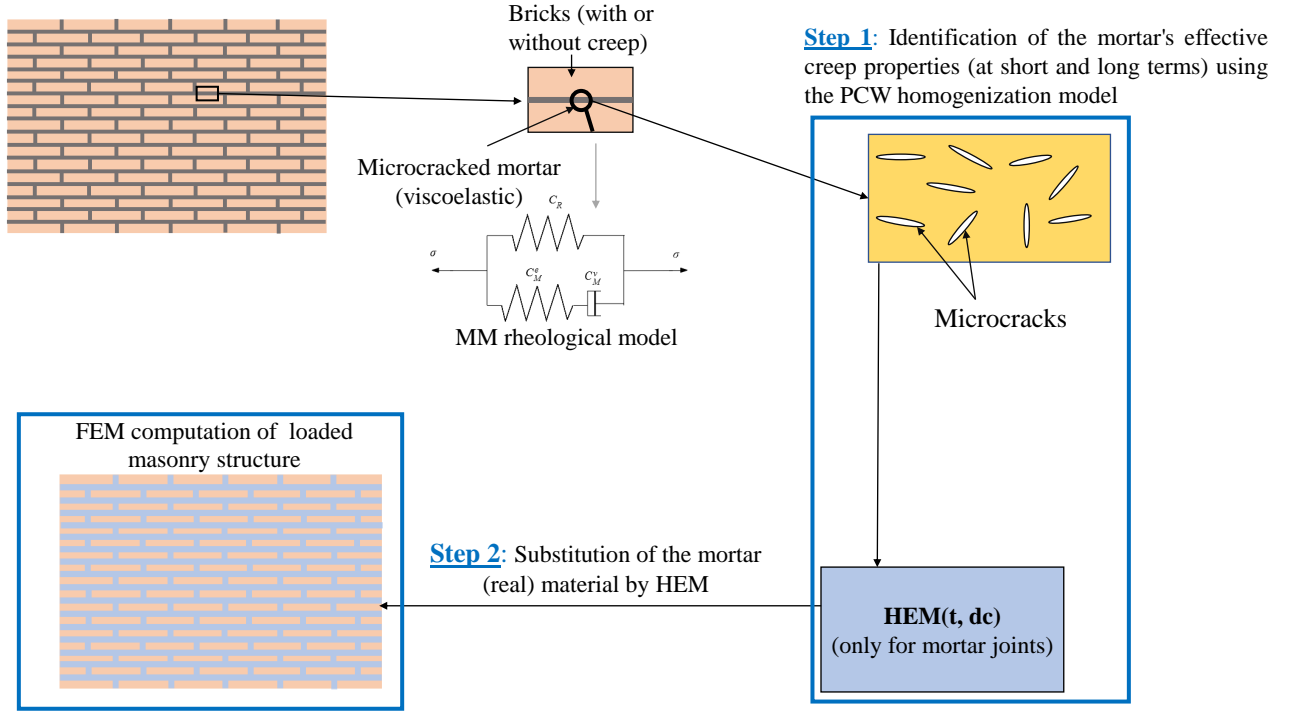


Figure 1: Principle of the proposed model : main steps

Hereafter, it is proposed to describe in more details the two steps on whose relies the proposed semi-numerical model.

### 2.1. Step 1: Rigorous homogenization of the microcracked viscoelastic mortar

At undamaged state, the mortar is assumed to be isotropic following the Generalized Maxwell Model (with one term) which constitutive law reads:

$$\mathbb{S}_M^v \boldsymbol{\sigma} + \mathbb{S}_M^e \dot{\boldsymbol{\sigma}} = \mathbb{S}_M^v \mathbb{C}_R^e \boldsymbol{\epsilon} + (\mathbb{I} + \mathbb{S}_M^e \mathbb{C}_R^e) \dot{\boldsymbol{\epsilon}} \quad (1)$$

The elastic and viscoelastic parts of the Maxwell part are given respectively by:

$$\mathbb{S}_M^e = \frac{1}{3k_M} \mathbb{J} + \frac{1}{2\mu_M} \mathbb{K} \quad , \quad \mathbb{S}_M^v = \frac{1}{\eta_M^s} \mathbb{J} + \frac{1}{\eta_M^d} \mathbb{K} \quad (2)$$

whereas the elastic stiffness of the spring reads:

$$\mathbb{C}_R^e = 3k_R \mathbb{J} + 2\mu_R \mathbb{K} \quad (3)$$

The spherical projector (fourth-order tensor) is denoted by  $\mathbb{J}$  and  $\mathbb{K} = \mathbb{I} - \mathbb{J}$  is the deviatoric projector.  $\mathbb{I}$  is the fourth-order identity tensor.  $k_\alpha$  and  $\mu_\alpha$  ( $\alpha = R, M$ ) are respectively the bulk and shear moduli of the springs.  $\eta_M^s$  and  $\eta_M^d$  represent respectively the bulk and shear viscosities of the dashpot.

Now assuming that mortar is microcracked with identical and randomly oriented cracks [36], two frictionless

crack states can be considered (open and closed). In the symbolic space, the mortar global behaviour is apparently elastic and its symbolic effective stiffness tensor  $\tilde{\mathbb{C}}^*$  can be expressed as:

$$\tilde{\mathbb{C}}^* = 3\tilde{k}_{PCW}^* \mathbb{J} + 2\tilde{\mu}_{PCW}^* \mathbb{K} \quad (4)$$

where  $\tilde{k}_{PCW}^*$  and  $\tilde{\mu}_{PCW}^*$  are respectively the effective symbolic bulk and shear moduli taking the following forms [21]:

$$\begin{aligned} \tilde{k}_{PCW}^* &= k_m^* \left( 1 - \frac{48d_c (1 - (\nu_m^*)^2)}{27(1 - 2\nu_m^*) + 16d_c(1 + \nu_m^*)^2} \right) \\ \tilde{\mu}_{PCW}^* &= \mu_m^* \left( 1 - \frac{480d_c (1 - \nu_m^*) (5 - \nu_m^*)}{675(2 - \nu_m^*) + 64d_c(4 - 5\nu_m^*)(5 - \nu_m^*)} \right) \end{aligned} \quad (5)$$

where

$$k_m^*(p) = k_R + \frac{1}{\frac{1}{k_M} + \frac{3}{p\eta_M^s}}, \quad \mu_m^*(p) = \mu_R + \frac{1}{\frac{1}{\mu_M} + \frac{2}{p\eta_M^d}}, \quad \nu_m^* = \frac{3k_m^* - 2\mu_m^*}{6k_m^* + 2\mu_m^*} \quad (6)$$

Here the subscript "m" refers to the undamaged mortar (matrix), whereas  $\nu_m^*$  is its symbolic Poisson's ratio. The damaged mortar symbolic Poisson's ratio can be deduced from symbolic bulk and shear modulus (equations (5)) as follows:

$$\tilde{\nu}_{PCW}^*(p, d_c) = \frac{3\tilde{k}_{PCW}^* - 2\tilde{\mu}_{PCW}^*}{6\tilde{k}_{PCW}^* + 2\tilde{\mu}_{PCW}^*} \quad (7)$$

The temporal expression of equation (7) is provided by the inverse Laplace-Carson transform [42]. Hereafter, we describe briefly the followed procedure allowing to identify the creep properties of the microcracked mortar at short and long terms based on theorems on the initial and final values given by:

$$\lim_{p \rightarrow 0} f^*(p) = \lim_{t \rightarrow \infty} f(t) \quad , \quad \lim_{p \rightarrow \infty} f^*(p) = \lim_{t \rightarrow 0} f(t) \quad (8)$$

### 2.1.1. Identification of the creep properties of the cracked mortar

In the symbolic space, the effective properties of the HEM owing to the PCW model (relations (5)) can be expanded to the first order around  $p = 0$  and at the vicinity of  $p = \infty$  (as shown respectively by relations (7) and (8) provided in paper [36]). On the other hand, as the mortar is characterized by a non-aging viscoelastic behaviour following at the undamaged state the MM's model, it can also be assumed to follow the same rheological model at its cracked state. It's properties at the global scale (in the symbolic space) can then be expressed by:

$$\begin{aligned} k_{MM}^* &= k_R(d_c) + \frac{pk_M(d_c)\eta_M^s(d_c)/3}{k_M(d_c) + p\eta_M^s(d_c)/3} \\ \mu_{MM}^* &= \mu_R(d_c) + \frac{p\mu_M(d_c)\eta_M^d(d_c)/2}{\mu_M(d_c) + p\eta_M^d(d_c)/2} \end{aligned} \quad (9)$$

whose series expansion around 0 and at the vicinity of  $\infty$  take respectively the forms provided by equations (11) and (12) in [36]. Besides, the equalities of the equations: (7)-a=(11)-a, (7)-b=(11)-b, (8)-a=(12)-a and (8)-b=(12)-b available in [36] allow to identify the HEM's symbolic parameters and hence its creep function  $\tilde{J}_{MM}$  given by equation (15) in [36] that depends on the crack density parameter  $d_c$  described hereafter.

### 2.1.2. Mortar's time-dependent crack density

Shrive et al. [44] proposed a power-law time evolution function for the mortar accumulated damage  $d_c$  according to the Weibull's failure rate function as:

$$d_c(t) = \sum_{i=t_0}^t \frac{100\eta}{\tau_D} \left( \frac{t_i}{\tau_D} \right)^n \quad (10)$$

$\tau_D$  is a constant referring to the time where most damage would occur. According to the damage scenario adopted by Shrive et al. [44], the coefficients are set to  $\tau_D = 800 \text{ days}$ ,  $\eta = 0.3$  and the exponent  $n$  is given by  $n = 10$ . The damage is assumed to start slowly at  $t_0 = 400 \text{ days}$  and to accelerate over time to attain 0.33 after 1000 *days* as shown on Figure-2.

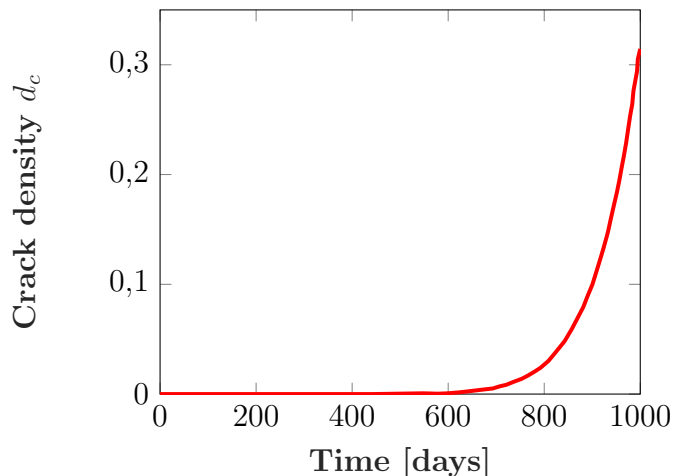


Figure 2: Nonlinear time-evolution of the crack density [44]

Other possible or more sophisticated damage scenarios [18] could be investigated in future works. As shown hereafter, only nonlinear time-evolution of damage ratio (equation (10)), is considered as a starting point allowing first illustration of the proposed semi-numerical model.

### 2.2. Step 2: Accurate full computation of the masonry

Instaed of using periodic homogenization technique that approaches the local behaviour of the masonry, we compute "exactly" (up to numerical error) its behaviour by modeling the full geometry of the masonry due to finite elements method using the Cast3M software [13]. This allows to get accurate responses at local and global scales. To achieve this step, we assume that masonry structure is composed by two homogeneous materials: bricks and HEM( $t, d_c$ ) defined in step-1 for the mortar (subsection (2.1)). Bricks are assumed to be undamaged without or with creep (following also the MM's model). Instantaneously, the brick's behaviour can be described by a time evolution Young's modulus  $E_b(t)$  and a constant Poisson's ratio  $\nu_b$ . According to the limits (see equation (20) in paper [36]) attained by the microcracked mortar's creep function (at the vicinity of 0 and infinity), the behaviour of the mortar can be assumed to be elastic and damaged at short and long terms. It's Young's modulus is given by:

$$\tilde{E}_{PCW}(t, d_c) = \frac{1}{\tilde{J}_{MM}(t, d_c)} \quad (11)$$

The proposed model can be applied to various masonry structures (masonry buildings or refractory linings). It improves the accuracy of previous models [36, 37, 40] even if it needs more computational capacity.

## 3. Illustrative example: case of a compressed masonry wall

As a first illustration of the relevance of proposed model, we investigate here the case of a compressed masonry wall as shown on Figure-3. Notice that all the computations have been carried out under plane stress assumption by using a quadratic element 'QUA8' with 8 nodes and a refined mesh elements using

the software Cast3M. We investigate the masonry creep phenomenon through the case of masonry panels subjected to constant force at selected points of the boundary (i.e. a sustained macroscopic stress). Since analytical solution does not exist for microcracked viscoelastic masonry, it is proposed firstly, similarly to the methodology followed in [36], to validate the proposed model by comparison with analytical solution available for an uncracked viscoelastic masonry wall (Figure-3(a)) provided by Cecchi and Sab [15]. The load case considered in Figure-3(b) is identical to that studied in [36]. It allows to investigate predictions of the semi-numerical model in terms of local mechanical responses even in the presence of creep in bricks.

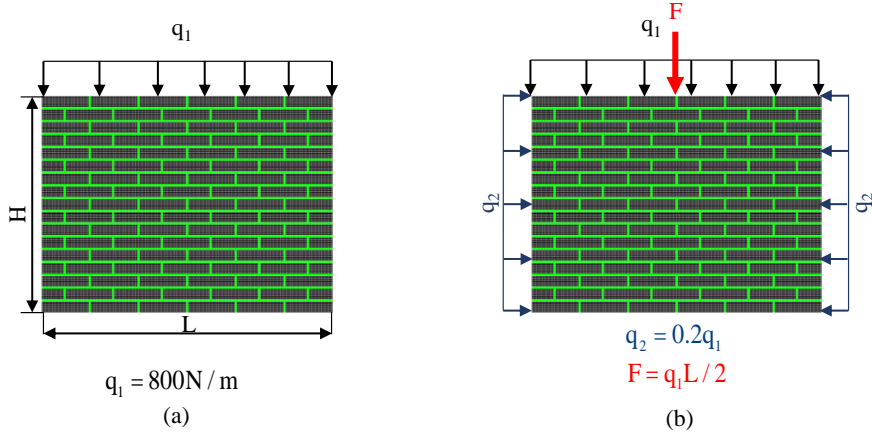


Figure 3: Masonry wall (with rigid (a) and elastic or viscoelastic (b) bricks) subjected to distributed loads: at the top (a) and two lateral edges with an additional concentrated load  $F$  (b)

### 3.1. Validation step: Comparison with analytical solution available for masonry with rigid bricks

This part aims to study the sensitivity of the herein proposed model to the mesh refinement and to validate it so that the obtained numerical solution is close to the analytical one related to the homogenized continuum model [3] in terms of the vertical displacement  $u_y$  when the mortar is assumed to be uncracked. Dimensions of the considered masonry panel are the following: length  $L = 1550 \text{ mm}$  and height  $H = 1040 \text{ mm}$ . Brick's dimensions are: length  $a = 250 \text{ mm}$ , height  $b = 50 \text{ mm}$  and thickness  $s = 120 \text{ mm}$ .  $e_h = e_v = 10 \text{ mm}$ , where  $e_h$  and  $e_v$  are respectively the thicknesses of the mortar joints in the horizontal and vertical directions. The wall is assumed to be submitted to a vertical distributed compressive load as shown on Figure-3(a). Bricks are rigid, while the mortar is considered to be undamaged and viscoelastic following the Zener rheological model with elastic and viscous properties provided in Table-1. The instantaneous Young's modulus  $E_0$

Table 1: Elastic and viscous properties of the undamaged mortar [10, 16]

$E_0(\text{MPa})$	$\nu_m$	$e_i$	$\tau_M(\text{days})$
7700	0.2	0.7602	7.1

for the MM's model is given by  $E_0 = E_M + E_R$ , where the relaxation  $E_M$  and spring's Young's modulus are given respectively by  $E_M = e_i E_0$  and  $E_R = (1 - e_i) E_0$  ( $e_i$  is a dimensionless parameter). Finally, the symbolic mortar's effective Poisson's ratio  $\tilde{\nu}_{PCW}$  is given by equation (18) [36]. When mortar is assumed to be uncracked ( $d_c = 0$ ), this equation provides a constant identical to  $\nu_m = 0.2$ . In this study, since damage is assumed to mainly concentrate in mortar joints by contrary to bricks which are assumed to be undamaged, the applied sustained stress is lower than the brick's compressive strength  $f_b$  but higher than the mortar's compressive strength. As mentioned by Cecchi and Tralli [17], the mortar is assumed to be of class M5. Accordingly, its compressive strength is equal to 5 MPa, however that of the brick is around 16 MPa following the Eurocode 6 equation:  $E_b = 4550\sqrt{f_b}$  [17].

Recall that, under in-plane stress assumption, the analytical solution of a vertically compressed homogeneous

plate which properties are derived from an analytical homogenization procedure by Cecchi and Sab research [15] reads:

$$u_y(x, H, t) = \frac{Q_1 H}{A_{2222}^F(t) \cdot L \cdot s} = \frac{q_1 H}{A_{2222}^F(t)} \quad (12)$$

where  $q_1 = Q_1/(Ls)$  is the pressure applied at the top of the wall,  $Q_1$  is the associated vertical distributed load and  $A_{ijkl}^F$  is the approximate homogenized relaxation coefficients estimated by the kinematically admissible solution [15]. In particular,  $A_{2222}^F$  takes the form provided by equation (28) in [36], where  $K_h(t) = \frac{E_m(t)}{(1+\nu_m)(1-2\nu_m)}$  is the bulk relaxation modulus of horizontal interfaces.

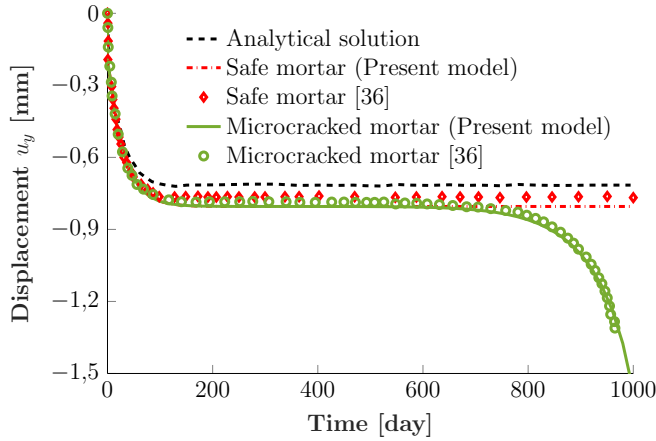


Figure 4: Temporal evolutions of the vertical displacement at the top of the wall

Notice here that the viscoelastic behaviours of the bed and head mortar joints are assumed to be coincident and defined by the following relaxation function (or instantaneous Young's modulus  $E_m(t) = \tilde{E}_{PCW}(t, d_c)$ ) and Poisson's ratio  $\nu_m(t) = \tilde{\nu}_{PCW}$ . Results provided by the semi-numerical model for masonry wall with undamaged and cracked mortar joints are depicted on Figure-4.

At the undamaged state, it can be observed that the semi-numerical solution is close to the analytical one (the maximum relative error is lower than 7%). Moreover, the semi-numerical solution is less rigid. This can be explained by the fact that the proposed model accounts for real thickness of the mortar joints ( $e_h = e_v = 10mm$ ) by contrary to the analytical solution which substitutes these joints by interfaces assuming that  $e_h = e_v \rightarrow 0$ . Besides, the analytical solution considers approximate expression for the homogenized relaxation coefficient  $A_{2222}^F$  under assumption of in-plane macroscopic strain [15]. Accordingly, the semi-numerical model can be considered to be more accurate than the analytical solution as it accounts for rigorously softening effect induced by finite (non-zero) thickness mortar joints. Notice that this numerical result is obtained for the following refinement mesh: 1000 elements for brick, 100 (300) for head (bed) mortar joint, which is retained below.

At the microcracked state, the mortar's Young's modulus follows evolution reported on Figure (14) [36]. Qualitatively, the evolution of the vertical displacement  $u_y$  on the top of the wall (continuous curve in Figure-4) shows similar trend as that observed for the panel with undamaged mortar till  $t = 600$  (days). The relative error between the semi-numerical and analytical solutions is lower than 7%. After that ( $600 < t \leq 1000$  days), the absolute value of the displacement  $u_y$  highly decreases. The error between semi-numerical solutions at undamaged and damaged states reach for example 19.36% at time  $t = 900$  days for a crack density equal to 0.2. This is consistent with the relaxation of the microcracked mortar's Young's modulus observed in Figure (14) [36].



### 3.2. Model's predictions for damaged masonry with elastic and viscoelastic bricks

In this section, it is proposed to investigate the local behaviour of a masonry wall (height =1040 mm, length=1550 mm) subjected to both vertical and lateral compressive distributed loads added to a concentrated load  $F$  applied on the top of the wall (at  $x = L/2$ ) as shown on Figure-3(b). The mortar, which properties at the undamaged state are given in Table-1, is assumed to be viscoelastic and damaged with frictionless open microcracks. The six parameters  $k_R, k_M, \eta_M^s, \mu_R, \mu_M, \eta_M^d$  characterizing the creep behaviour of the microcracked mortar are identified following the step-1 described in Section-2.1 and provided in Table-2.

Table 2: Estimates for the mortar's creep coefficients following the PCW model (case of open cracks [36])

$k_R (MPa)$	$k_M (MPa)$	$\eta_s (MPa.s)$
$-1025.81 + \frac{1442.55}{0.703125 + d_c}$	$-3251.97 + \frac{4573.08}{0.703125 + d_c}$	$-5.98466 \cdot 10^9 + \frac{8.41593 \cdot 10^9}{0.703125 + d_c}$
$\mu_R (MPa)$	$\mu_M (MPa)$	$\eta_d (MPa.s)$
$-769.358 + \frac{2028.58}{1.31836 + d_c}$	$-2438.98 + \frac{6430.89}{1.31836 + d_c}$	$-2.99233 \cdot 10^9 + \frac{7.88993 \cdot 10^9}{1.31836 + d_c}$

This part makes comparison between masonry with elastic and viscoelastic bricks which properties are given in Table-3.

Table 3: Brick's elastic and viscous properties [10, 16]

$E_0 (MPa)$	$\nu_b$	$e_i$	$\tau_M (days)$
17100	0.15	0.5327	33.8

Recall that, according to the MM's model, the brick's Young's modulus  $E_b(t) = 1/J_{MM}^b(t)$  is time-dependent as shown in equation (21) [36], where  $J_{MM}^b$  is the brick's creep function. Notice that the modulus  $E_b(t)$  tends towards constants either at short ( $t \rightarrow 0$ ) or long ( $t \rightarrow \infty$ ) terms. As a whole, it is observed that the semi-numerical model's predictions are consistent with the increase of the damage level with time, the significant decrease of the mortar's Young's modulus and relaxation of the brick's Young's modulus when the creep is accounted for.

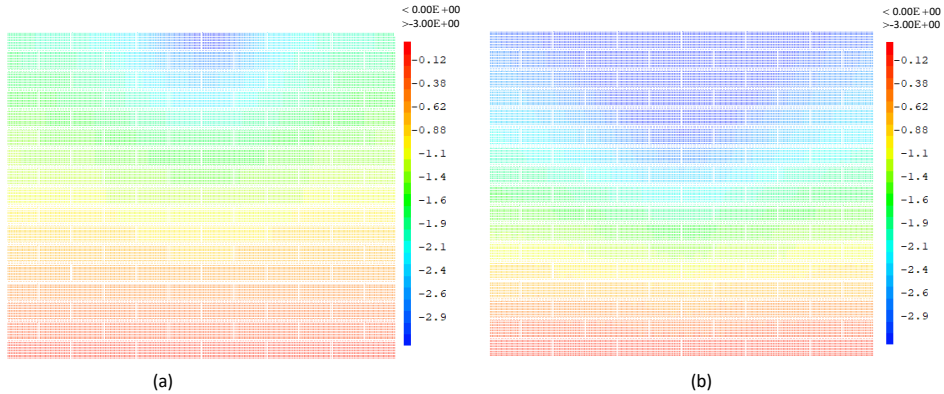


Figure 5: Comparison between masonry with elastic (a) and viscoelastic (b) bricks: displacement snapshots throughout the wall at time  $t = 900 \text{ days}$

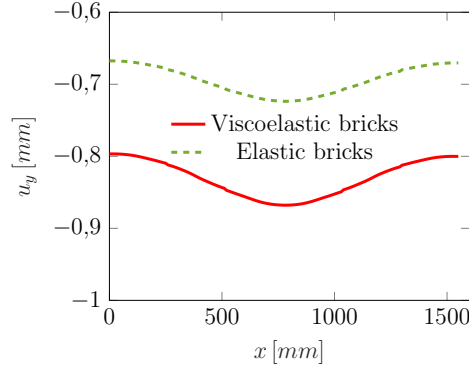


Figure 6: Comparison between masonry with elastic (a) and viscoelastic (b) bricks: evolution of the vertical displacement along the x axis in the middle height of the wall at time  $t = 900 \text{ days}$

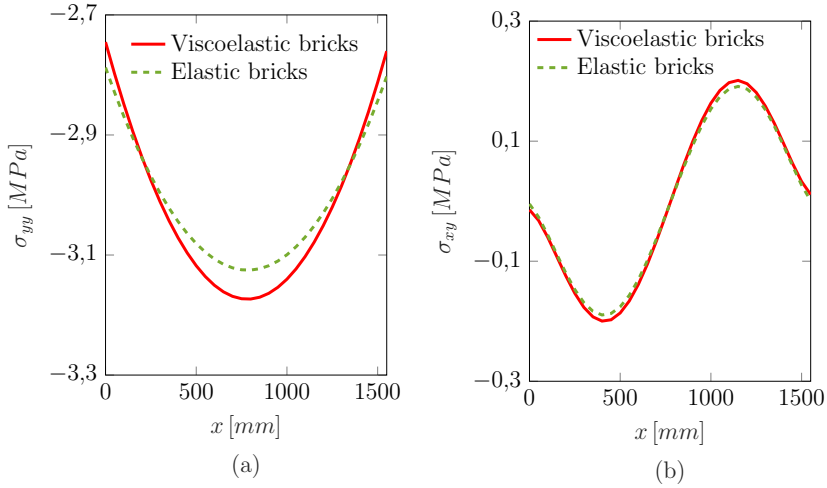


Figure 7: Comparison between masonry with elastic (a) and viscoelastic (b) bricks: evolution of normal (a) and shear (b) stresses along the x axis in the middle height of the wall at time  $t = 900 \text{ days}$

Since the tertiary creep of the mortar starts beyond time  $t = 700 \text{ days}$  (as shown in Figure (12) [36]), we propose in the following to investigate the behaviour of the masonry walls at time  $t = 900 \text{ days}$ . The spatial distributions of the vertical displacement  $u_y$  throughout walls made of viscoelastic microcracked mortar and elastic and viscoelastic bricks are depicted respectively in Figure-5(a) et 5(b). For the two cases, it can be observed that  $u_y$  is negativ and its absolute value attains its maximum around the application point of the concentrated load  $F$  at the top of the wall. This trend is confirmed by Figure-6 reporting the evolutions along the x axis of the displacement  $u_y$  at the middle height of the walls. Quantitatively, either on Figure-5 or 6, it is possible to observe that the absolute value of the displacement is higher when bricks are viscoelastic. For example, the relative error between the two displacements (with and without brick's creep) at the middle height at  $x = L/2$  is about 23.25%. This is consistent with the softening effect induced by the relaxation of the brick's Young's modulus  $E_b(t)$  observed in Figure (14) [36].

Figure-7 (Figure-8) illustrates evolutions of normal  $\sigma_{yy}$  and shear  $\sigma_{xy}$  stresses (strains  $\varepsilon_{yy}$  and  $\varepsilon_{xy}$ ) along the x axis at the middle height of the wall ( $y = H/2$ ). Quantitatively, normal stress is negativ showing that masonry panel is submitted locally to compression which attain its maximum around the application point of the concentrated load  $F$ . It can also be noticed that the absolute value of  $\sigma_{yy}$  is higher for masonry with

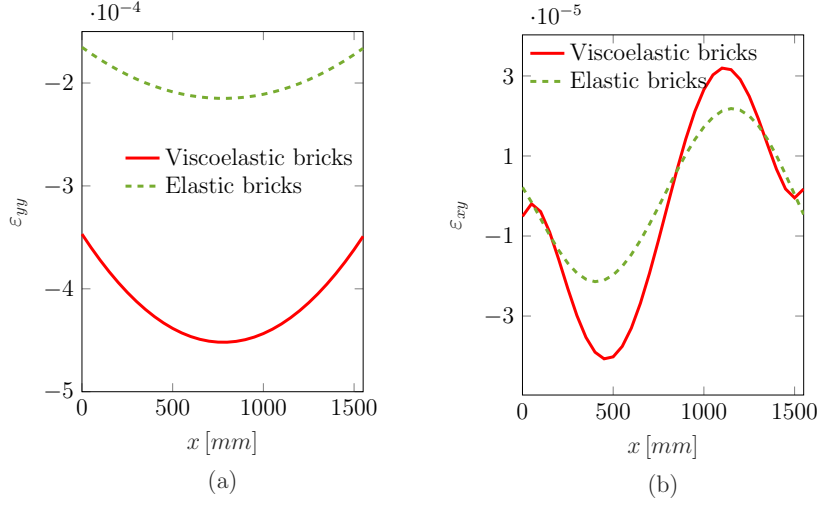


Figure 8: Comparison between masonry with elastic (a) and viscoelastic (b) bricks: evolution of normal (a) and shear (b) strains along the x axis in the middle height of the wall at time  $t = 900$  days

viscoelastic bricks. The maximum relative error between stresses can reach 2.66% and 6.45%, respectively for  $\sigma_{yy}$  and  $\sigma_{xy}$  showing that the presence of creep in bricks increases the stress level in the masonry and could accordingly accelerate the failure phenomena around the application point of the load F. On the other hand, shear stresses in masonry panel with viscoelastic bricks are almost equal to  $\sigma_{xy}$  in the panel with elastic bricks even if they are slightly higher. Notice here that shear stresses are negligible by comparison to normal stresses which is consistent with the applied boundary conditions. Besides, the proposed semi-numerical model shows more significant quantitative differences for the strain field when comparing panels with elastic and viscoelastic bricks. Indeed relative error between strains can reach 72.55% and 40.8%, respectively for  $\epsilon_{yy}$  and  $\epsilon_{xy}$ . It can then be deduced that creep of bricks highly increases strains in masonry which is consistent with the additional softening induced by the relaxation of the brick's Young's modulus. These results give more insight to the creep effects of bricks.

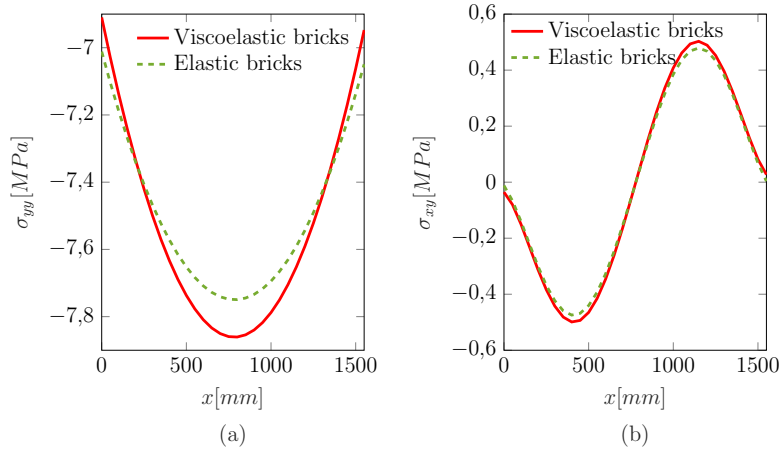


Figure 9: Comparison between masonry panels with elastic and viscoelastic bricks upon activation of tertiary creep of mortar: evolution of the normal  $\sigma_{yy}$  (a) and shear  $\sigma_{xy}$  (b) stresses along the x axis in the middle height of the wall at time  $t = 900$  days

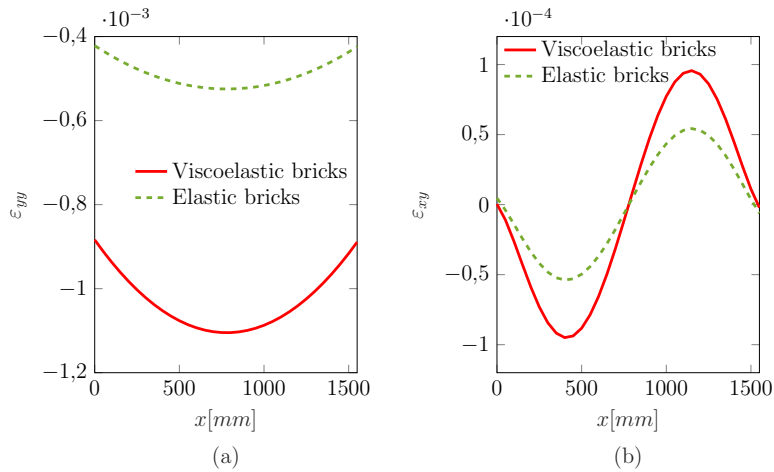


Figure 10: Comparison between masonry panels with elastic and viscoelastic bricks upon activation of tertiary creep of mortar: evolution of the normal  $\varepsilon_{yy}$  (a) and shear  $\varepsilon_{xy}$  (b) strains along the  $x$  axis in the middle height of the wall at time  $t = 900$  days

To emphasize the effect of brick's creep, we investigate in the following the case of walls submitted to higher sustained pressure ( $q_1 = 2000$  N/m). It can be observed in Figure-9 that local (normal and shear) stresses are increased in the walls. Moreover, normal stress exceeds  $5$  MPa (the compressive strength of the mortar) at the level of the middle height of the wall (either with elastic or viscoelastic bricks) mainly around the application point of the concentrated load which is a potential area of failure. Similar trends are observed for the normal and shear strains (Figure-10). The former is highly increased compared to results reported in Figure-8. Again, it can be observed that strains in the wall with elastic bricks are negligible by comparison to those in the wall with viscoelastic bricks mainly in the area around the application point of the load  $F$ . Indeed, the relative errors reach respectively 70.935% and 55.61% at  $x = L/2$ . These trends are in well agreement with those observed in Figure-7 and 8, which confirm the non-negligible softening effect induced in the masonry by the presence of creep in bricks.

#### 4. Conclusions and perspectives

This paper develops a semi-numerical model coupling Griffith's theory to an accurate analytical homogenization model (the PCW scheme) and finite elements method in order to assess accurately the microcracked masonry behaviour. It accounts for many parameters: mortar joint's thickness, creep of both masonry constituents (brick and mortar), interactions of microcracks, their spatial distribution and state (open). The sensitivity of this model to the mesh refinement was investigated and validated due to a comparison with analytical solution available for homogeneous plate [15] submitted to vertical compressive load. For the sake of simplicity and as a first illustration, this model was applied to a compressed masonry with elastic and viscoelastic bricks. Results show the significant softening effect induced by the presence of microcracks on the masonry mechanical response added to the relaxation of the mortar's Young's modulus. Accounting for creep of bricks accentuates this softening. Risk of failure is then increased by two factors: presence of open frictionless microcracks in the mortar and creep of bricks. In this work, it can be mentioned that the proposed model could be improved by considering interfaces between bricks and mortar and transition between microcracks states (open and closed) in order to investigate damage propagation in a thermodynamics framework [20] or by a stress criterion [26]. Moreover, it could be interesting to account for presence of cracks in bricks and to extend this model to the case of anisotropic mortar containing parallel cracks [5, 53]. At last, considering the masonry ageing phenomenon [4] and thermal loading will enrich the proposed model. These perspectives are left for further investigations.

## References

- [1] A. AHMED ET K. SHAHZADA, *Seismic vulnerability assessment of confined masonry structures by macro-modeling approach*, in Structures, vol. 27, Elsevier, 2020, p. 639–649.
- [2] F. P. ALMEIDA ET P. B. LOURENÇO, *Three-dimensional elastic properties of masonry by mechanics of structure gene*, International Journal of Solids and Structures, 191 (2020), p. 202–211.
- [3] D. BARALDI ET A. CECCHI, *Discrete element model for in-plane loaded viscoelastic masonry*, International Journal for Multiscale Computational Engineering, 12 (2014), p. 155–175.
- [4] J.-F. BARTHÉLÉMY, A. GIRAUD, F. LAVERGNE ET J. SANAHUJA, *The Eshelby inclusion problem in ageing linear viscoelasticity*, International Journal of Solids and Structures, 97 (2016), p. 530–542.
- [5] J. BLUTHÉ, B. BARY ET E. LEMARCHAND, *Closure of parallel cracks: Micromechanical estimates versus finite element computations*, European Journal of Mechanics-A/Solids, 81 (2020).
- [6] E. BONETTI, G. BONFANTI, F. LEBON ET R. RIZZONI, *A model of imperfect interface with damage*, Meccanica, 52 (2017), p. 1911–1922.
- [7] M. BORNERT, T. BRETHERAU ET P. GILORMINI, *Homogénéisation en mécanique des matériaux, Tome 1: Matériaux aléatoires élastiques et milieux périodiques*, Hermes science, 2001.
- [8] D. BRICCOLA ET M. BRUGGI, *Analysis of 3d linear elastic masonry-like structures through the api of a finite element software*, Advances in Engineering Software, 133 (2019), p. 60–75.
- [9] D. BRICCOLA, M. BRUGGI ET A. TALIERCIO, *Assessment of 3d linear elastic masonry-like vaulted structures*, in Key Engineering Materials, vol. 817, Trans Tech Publ, 2019, p. 50–56.
- [10] J. BROOKS, *Composite modelling of masonry deformation*, Materials and structures, 23 (1990), p. 241–251.
- [11] B. BUDIANSKY ET R. J. O’CONNELL, *Elastic moduli of a cracked solid*, International journal of Solids and structures, 12 (1976), p. 81–97.
- [12] C. CASAPULLA, A. MAIONE, L. ARGIENTO ET E. SPERANZA, *Corner failure in masonry buildings: an updated macro-modeling approach with frictional resistances*, European Journal of Mechanics-A/Solids, 70 (2018), p. 213–225.
- [13] CAST3M, <http://www-cast3m.cea.fr>, 2020.
- [14] P. P. CASTAÑEDA ET J. R. WILLIS, *The effect of spatial distribution on the effective behavior of composite materials and cracked media*, Journal of the Mechanics and Physics of Solids, 43 (1995), p. 1919–1951.
- [15] A. CECCHI ET K. SAB, *A comparison between a 3d discrete model and two homogenised plate models for periodic elastic brickwork*, International journal of solids and structures, 41 (2004), p. 2259–2276.
- [16] A. CECCHI ET A. TALIERCIO, *A comparison between numerical and analytical homogenized models for visco-elastic brickwork*, in XXI Congresso AIMETA Associazione Italiana di Meccanica Teorica e Applicata, 2013, p. 1–10.
- [17] A. CECCHI ET A. TRALLI, *A homogenized viscoelastic model for masonry structures*, International Journal of Solids and Structures, 49 (2012), p. 1485–1496.
- [18] K. CHAN, S. BODNER, A. FOSSUM ET D. MUNSON, *A constitutive model for inelastic flow and damage evolution in solids under triaxial compression*, Mechanics of Materials, 14 (1992), p. 1–14.
- [19] K.-K. CHOI, S. L. LISSEL ET M. M. REDA TAHA, *Rheological modelling of masonry creep*, Canadian Journal of Civil Engineering, 34 (2007), p. 1506–1517.
- [20] L. DORMIEUX ET D. KONDO, *Stress-based estimates and bounds of effective elastic properties: the case of cracked media with unilateral effects*, Computational Materials Science, 46 (2009), p. 173–179.
- [21] L. DORMIEUX, D. KONDO ET F.-J. ULM, *Microporomechanics*, John Wiley & Sons, 2006.
- [22] T. FAN, J. KIM, M. REDA TAHA ET N. SHRIVE, *A three dimensional finite element model simulating damage and creep interaction in masonry*, in Proceedings of 11th Canadian Masonry Symposium, 2009, p. 551–558.
- [23] S. IGNOUL, L. SCHUEREMANS, J. TACK, L. SWINNEN, S. FEYTONS, L. BINDA, D. VAN GEMERT ET K. VAN BALEN, *Creep behavior of masonry structures—failure prediction based on a rheological model and laboratory tests*, Structural Analysis of Historical Constructions, (2006), p. 913–920.
- [24] L. A. S. KOURIS, D. A. BOURNAS, O. T. AKINTAYO, A. A. KONSTANTINIDIS ET E. C. AIFANTIS, *A gradient elastic homogenisation model for brick masonry*, Engineering Structures, 208 (2020).
- [25] D. LENCZNER ET J. SALAHUDDIN, *Creep and moisture movements in brickwork wall*, in Proceedings of the 4th International Brick Masonry Conference, Bruges, Belgium, 1976, p 2.
- [26] T. MASSART, R. PEERLINGS ET M. GEERS, *Structural damage analysis of masonry walls using computational homogenization*, International journal of damage mechanics, 16 (2007), p. 199–226.
- [27] L. NAZARENKO, H. STOLARSKI ET H. ALTENBACH, *A statistical interphase damage model of random particulate composites*, International Journal of Plasticity, 116 (2019), p. 118–142.
- [28] B. NEDJAR ET R. LE ROY, *An approach to the modeling of viscoelastic damage. application to the long-term creep of gypsum rock materials*, International Journal for Numerical and Analytical Methods in Geomechanics, 37 (2013), p. 1066–1078.
- [29] L. NGUYEN, STAND DORMIEUX, *Viscoelastic properties of transversely isotropic micro-cracked materials*, International Journal of Damage Mechanics, 25 (2016), p. 141–152.
- [30] S. NGUYEN, *Generalized Kelvin model for micro-cracked viscoelastic materials*, Engineering Fracture Mechanics, 127 (2014), p. 226–234.
- [31] S. NGUYEN ET L. DORMIEUX, *Propagation of micro-cracks in viscoelastic materials: Analytical and numerical methods*, International Journal of Damage Mechanics, 24 (2015), p. 562–581.
- [32] S. NGUYEN, L. JEANNIN, L. DORMIEUX ET F. RENARD, *Fracturing of viscoelastic geomaterials and application to sedimentary layered rocks*, Mechanics Research Communications, 49 (2013), p. 50–56.

- [33] S. T. NGUYEN, L. DORMIEUX, Y. L. PAPE ET J. SANAHUJA, *A Burger model for the effective behavior of a microcracked viscoelastic solid*, International Journal of Damage Mechanics, 20 (2011), p. 1116–1129.
- [34] B. PANTÒ, L. SILVA, G. VASCONCELOS ET P. LOURENÇO, *Macro-modelling approach for assessment of out-of-plane behavior of brick masonry infill walls*, Engineering Structures, 181 (2019), p. 529–549.
- [35] C. PIAN, E. V. MUHO, G. LU ET J. QIAN, *Application of asymptotic expansion homogenization in vibration analysis of masonry structures using finite elements*, Mechanics Research Communications, 104 (2020), p. 103481.
- [36] A. REKIK, *Rigorous Estimates for Effective Creep-coefficients of Microcracked Masonry Accounting for Cracks Interactions*, Periodica Polytechnica Civil Engineering, 64 (2020), p. 557–578.
- [37] A. REKIK ET A. GASSER, *Numerical homogenization model for effective creep properties of microcracked masonry*, International Journal of Solids and Structures, 102 (2016), p. 297–320.
- [38] A. REKIK ET F. LEBON, *Homogenization methods for interface modeling in damaged masonry*, Advances in Engineering Software, 46 (2012), p. 35–42.
- [39] A. REKIK ET F. LEBON, *Micromodeling*, in Numerical Modeling of Masonry and Historical Structures, Elsevier, 2019, p. 295–349.
- [40] A. REKIK, T. T. N. NGUYEN ET A. GASSER, *Multi-level modeling of viscoelastic microcracked masonry*, International Journal of Solids and Structures, 81 (2016), p. 63–83.
- [41] E. Y. SAYED-AHMED, N. G. SHRIVE ET D. TILLEMANN, *Creep deformation of clay masonry structures: a parametric study*, Canadian Journal of Civil Engineering, 25 (1998), p. 67–80.
- [42] R. A. SCHAPERY, *Approximation methods of transform inversion for viscoelastic stress analysis*, Proc Fourth USNat Congr Appl Mech, 1962, 2 (1962), p. 1075.
- [43] I. SEVOSTIANOV, V. LEVIN ET E. RADI, *Effective properties of linear viscoelastic microcracked materials: Application of Maxwell homogenization scheme*, Mechanics of Materials, 84 (2015), p. 28–43.
- [44] N. SHRIVE ET M. R. TAHA, *Effects of creep on new masonry structures*, Learning From Failure, Long-Term Behaviour of Heavy Masonry Structures, (2008), p. 83–108.
- [45] L. C. SILVA, P. B. LOURENÇO ET G. MILANI, *Derivation of the out-of-plane behaviour of masonry through homogenization strategies: micro-scale level*, Computers & Structures, 209 (2018), p. 30–43.
- [46] M. R. TAHA ET N. SHRIVE, *A model of damage and creep interaction in a quasi-brittle composite material under axial loading*, Journal of Mechanics, 22 (2006), p. 339–347.
- [47] A. TALIERCIO, *Closed-form expressions for the macroscopic in-plane elastic and creep coefficients of brick masonry*, International Journal of Solids and Structures, 51 (2014), p. 2949–2963.
- [48] A. TALIERCIO ET E. PAPA, *Modelling of the long-term behaviour of historical masonry towers*, Learning from Failure: Long-term Behaviour of Heavy Masonry Structures, WIT Press, Southampton, UK, (2008), p. 153–173.
- [49] E. VERSTRYNGE, L. SCHUEREMANS ET D. VAN GEMERT, *Time-dependent mechanical behavior of lime-mortar masonry*, Materials and structures, 44 (2011), p. 29–42.
- [50] M. WEBER, K. THOMA ET J. HOFMANN, *Finite element analysis of masonry under a plane stress state*, Engineering Structures, 226 (2021).
- [51] J. YACILA, G. CAMATA, J. SALSAVILCA ET N. TARQUE, *Pushover analysis of confined masonry walls using a 3d macro-modelling approach*, Engineering Structures, 201 (2019).
- [52] T. ZAHRA ET M. DHANASEKAR, *A generalised damage model for masonry under compression*, International Journal of Damage Mechanics, 25 (2016), p. 629–660.
- [53] Q.-Z. ZHU, S.-S. YUAN ET J.-F. SHAO, *Bridging meso-and microscopic anisotropic unilateral damage formulations for microcracked solids*, Comptes Rendus Mécanique, 345 (2017), p. 281–292.